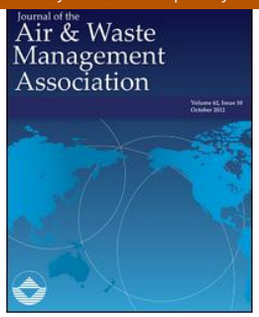

Journal of the Air & Waste Management Association

ISSN: 1096-2247 (Print) 2162-2906 (Online) Journal homepage: http://www.tandfonline.com/loi/uawm20

Feasibility of coupling a thermal/optical carbon analyzer to a quadrupole mass spectrometer for enhanced $PM_{2.5}$ speciation

Gustavo M. Riggio, Judith C. Chow, Paul M. Cropper, Xiaoliang Wang, Reddy L. N. Yatavelli, Xufei Yang & John G. Watson

To cite this article: Gustavo M. Riggio, Judith C. Chow, Paul M. Cropper, Xiaoliang Wang, Reddy L. N. Yatavelli, Xufei Yang & John G. Watson (2017): Feasibility of coupling a thermal/optical carbon analyzer to a quadrupole mass spectrometer for enhanced $PM_{2.5}$ speciation, Journal of the Air & Waste Management Association, DOI: 10.1080/10962247.2017.1394928

To link to this article: http://dx.doi.org/10.1080/10962247.2017.1394928

Accepted author version posted online: 09 Nov 2017.

Feasibility of Coupling a Thermal/Optical Carbon Analyzer to a Quadrupole Mass Spectrometer for Enhanced $PM_{2.5}$ Speciation

Gustavo M. Riggio, Desert Research Institute, Reno, NV, USA

Judith C. Chow, Desert Research Institute, Reno, NV, USA, State Key Laboratory of Loess and Quaternary Geology (SKLLQG), Institute of Earth Environment, Chinese Academy of Sciences, Xi'an, People's Republic of China

Paul M. Cropper, Desert Research Institute, Reno, NV, USA

Xiaoliang Wang, Desert Research Institute, Reno, NV, USA

Reddy L. N. Yatavelli, Air Resources Board, El Monte, CA, USA

Xufei Yang Montana Tech of the University of Montana, Butte, MT, USA

John G. Watson, Desert Research Institute, Reno, NV, USA, State Key Laboratory of Loess and Quaternary Geology (SKLLQG), Institute of Earth Environment, Chinese Academy of Sciences, Xi'an, People's Republic of China*

*Corresponding Author. Email: John.Watson@dri.edu

Abstract

A thermal/optical carbon analyzer (TOA), normally used for quantification of organic carbon (OC) and elemental carbon (EC) in $PM_{2.5}$ speciation networks, was adapted to direct thermally-evolved gases to an electron impact quadrupole mass spectrometer (QMS), creating a TOA-

QMS. This approach produces spectra similar to those obtained by the Aerodyne Aerosol Mass Spectrometer (AMS), but the ratios of the mass to charge (*m/z*) signals differ and must be re-measured using laboratory-generated standards. Linear relationships are found between TOA-QMS signals and ammonium (NH_4^+), nitrate (NO_3^-), and sulfate (SO_4^{2-}) standards. For ambient samples, however, positive deviations are found for SO_4^{2-}, compensated by negative deviations for NO_3^-, at higher concentrations. This indicates the utility of mixed-compound standards for calibration or separate calibration curves for low and high ion concentrations. The sum of the QMS signals across all *m/z* after removal of the NH_4^+, NO_3^-, and SO_4^{2-} signals was highly correlated with the carbon content of oxalic acid ($C_2H_2O_4$) standards. For ambient samples, the OC derived from the TOA-QMS method was the same as the OC derived from the standard IMPROVE_A TOA method. This method has the potential to reduce complexity and costs for speciation networks, especially for highly polluted urban areas such as those in Asia and Africa.

Implications: Ammonium, nitrate, and sulfate can be quantified by the same thermal evolution analysis applied to organic and elemental carbon. This holds the potential to replace multiple parallel filter samples and separate laboratory analyses with a single filter and a single analysis to account for a large portion of the $PM_{2.5}$ mass concentration.

Keywords: $PM_{2.5}$ Speciation, Material Balance, Thermal Analysis, Quartz-Fiber Filter, Mass Spectra

Introduction

Urban and non-urban $PM_{2.5}$ speciation networks in the U.S. (Solomon et al., 2014) and elsewhere measure major chemical components: 1) elements by x-ray fluorescence (Watson et al., 1999); 2) water-soluble ammonium (NH_4^+), nitrate (NO_3^-), sulfate (SO_4^{2-}), chloride (Cl^-), sodium (Na^+), and potassium (K^+) by ion chromatography (IC) (Chow and Watson, 1999, 2017); and 3) organic carbon (OC) and elemental carbon (EC) with a thermal/optical analyzer (TOA) (Chow et al., 1993b; 2007; 2011). With appropriate weighting for unmeasured hydrogen (H) and oxygen (O) components in geological material and organic matter (OM), the $PM_{2.5}$ gravimetric mass (Watson et al., 2017) can be reproduced with reasonable accuracy (Chow et al., 2015a). Measurements of these major components allow $PM_{2.5}$ to be attributed to source types and permit the tracking of air quality improvements with emission reductions (Chen et al., 2012; Murphy et al., 2011). Speciation measurements also allow adverse effects on human health (Grahame et al., 2014; Pope and Dockery, 2006), visibility (Watson, 2002), and climate (Fiore et al., 2015) to be related to aerosol chemistry.

Speciation networks currently acquire $PM_{2.5}$ deposits on different filters sampled in parallel that are then analyzed by several laboratory methods (Chow and Watson, 2013; Hidy et al., 2017). This approach produces accurate and precise concentrations, and allows for more complete characterization of new or archived filters (Watson et al., 2016). The cost and complexity of collecting on multiple filters for multiple types of analysis may preclude its application in resource-limited situations, such as those found in rapidly-industrializing countries of Asia and Africa that experience some of the highest $PM_{2.5}$ levels in the world (Lozano et al.,

2012). In these cases, sacrificing some accuracy and precision for an improved understanding of excessive concentrations is better than no information. With this need in mind, this work demonstrates the feasibility of extending the TOA measurement of OC and EC to quantification of NH_4^+, NO_3^-, and SO_4^{2-} on the same quartz-fiber filter sample. Cost-reductions may be possible due to the use of fewer filters and laboratory instruments. This is accomplished by using an electron ionization-quadrupole mass spectrometer (EI-QMS) to obtain mass spectra of the thermally-evolved aerosol (Riggio, 2015). This modification is termed the TOA-QMS.

Methodology

TOA-QMS Setup

Previous work (Diab et al., 2015; Grabowsky et al., 2011) demonstrated that a portion of the thermally-evolved gases from a TOA could be routed to a photo-ionization time-of-flight mass spectrometer (PI-TOF-MS) to acquire mass spectra on thousands of different organic compounds, resulting in thermal/spectral patterns that were better indicators of contributing sources than the seven thermal carbon fractions obtained from the IMPROVE_A carbon analysis protocol (Chow et al., 2007). A modest approach is taken here in which a more cost-effective and practical EI-QMS (Model MSD 5975, Agilent Technologies, Santa Clara, CA) is used as the detector. This EI-QMS employs an electron multiplier tube (EMT) for ion detection at mass to charge ratios (*m/z*) ranging from 10 to 450, with a complete spectrum generated every 1.2 seconds. The EI-QMS output is related to the ion current. Here the term *m/z signal* represents the output generated by the EI-QMS with the unit of photomultiplier counts/second (c/s).

Under normal TOA operation, a particle laden quartz-fiber filter punch (~ 0.5 cm^2) is heated in a sample oven following the IMPROVE_A protocol (Chow et al., 2007). The thermally-evolved gaseous products are passed through a manganese dioxide (MnO_2) oxidation reactor, yielding carbon dioxide (CO_2), followed by reduction to methane (CH_4) by hydrogen (H_2) on a nickel (Ni) catalyst. The CH_4 is quantified by a calibrated flame ionization detector (FID). Figure 1 illustrates modifications made to a DRI Model 2001 TOA (Atmoslytics, Calabasas, CA) to create the TOA-QMS. To demonstrate feasibility, the MnO_2 and Ni reactors were removed, although when put into practice two parallel streams would be used, as shown by Grabowsky et al. (2011). To reduce air infiltration during sample insertion, the system pressure was increased (from 1.35×10^5 to 1.7×10^5 Pa), and an argon sheath was placed at the interface of the sample pushrod before the oven to reduce O_2 content (from 15.5 to 8.5 ppm). Minimizing O_2 in the ultrapure (99.999%) helium (He) carrier gas reduces the reactions of O_2 with desorbed organic compounds that reduce sensitivity and parent molecule signatures. To minimize condensation of the evolved gases, the micro-volume connector and micro-metering valve were placed in an enclosed heated box (210 ^oC), connected by a heated (220 ^oC) fused silica capillary to the EI-QMS inlet (230 ^oC). Grabowsky et al. (2011) found that this differential heating reduced the condensation of volatile compounds along the capillary and at the EI-QMS inlet. The QMS flow rate was controlled to ~2 mL min^{-1} by a micro-metering valve.

The IMPROVE_A temperature protocol was also simplified for these feasibility tests, as shown in Figure 2a, using 580 °C and 840 °C temperature steps (with a starting temperature of 80 °C), the highest temperatures in the He and He/O_2 carrier gases, respectively, achieved in the protocol. The thermal fragmentation oven obtains molecular fragments similar to those achieved

by the widely-used Aerodyne Research Inc. (Billerica, MA) Electron Impact - Aerosol Mass Spectrometer (EI-AMS) (Jayne et al., 2000) that uses a QMS for detection.

Chemical identification of desorbed molecules was made at 10 minute intervals for temperatures of: 1) 80 °C to remove water and adsorbed volatile organic compounds (VOCs); 2) 580 °C to desorb and pyrolyze molecules from the aerosol deposit; and 3) 840 °C to quantify additional compounds that do not evolve at 580 °C. A 5% CO_2/ 95 % He mixture was injected as an internal standard using a six port injection valve with a 1 ml sample loop at the end of each run. The use of CO_2 as the internal standard instead of CH_4 (the original TOA internal standard gas) minimizes interferences between the *m/z* signals observed from the fragmentation of O_2 (*m/z*=16 for O^+) and CH_4 (*m/z*=16 for CH_4^+). Unit mass resolution is used to quantify NH_4^+, NO_3^-, SO_4^{2-}, and OC, similar to the approach used with the EI-AMS. Figure 2a shows the QMS integrated *m/z* signal at the different temperatures for a biomass burning sample, with most of the detected signal evolving at 580 ^oC. A mass spectrum of the same sample from *m/z* 10 to 250 averaged from 900 to 1500 seconds is shown in Figure 2b. Major species are shown with a downward arrow at *m/z* of 27, 39, 44, 91, and 115. The *m/z* 27 and 39 signals may represent alkenyl carbocation, while *m/z* 44 may represent CO_2, C_3H_8 and/or C_2H_4O. Other *m/z* signals may represent long hydrocarbon chains.

Calibration Methods

The EI-AMS calibration approach of Allan et al. (2004) was followed to obtain relative ionization efficiencies (RIE) that relate the mass spectra to chemical concentrations. Weighed amounts of ammonium nitrate (NH_4NO_3) and ammonium sulfate ($(NH_4)_2SO_4$) were dissolved in

distilled-deionized water, while weighed amounts of oxalic acid (C□H□O□, OM/OC=3.36) were dissolved in isopropanol. $C_2H_2O_4$ was chosen to represent OC since it is a major primary component of biomass burning (Yang et al., 2009) and is commonly found in atmospheric aerosols (Kerminen et al., 2000). In practice, a broader array of organic compounds would be used, but this single compound is sufficient for feasibility testing. In addition, testing of inorganic compounds containing water-soluble potassium, sodium, and chloride would close the gap needed to analyze samples from current chemical speciation networks. Aerosols were created from these solutions with a constant output atomizer (TSI, Model 3076) fed by a zero-air generator (Environics, Model 7000). The solvent associated with the particles was removed by passing the aerosol over activated charcoal for the organics and over silica gel beads for the inorganics prior to being drawn into a Teflon-coated chamber (Chow et al., 1993a) and sampled onto five parallel pre-fired (~900 ^{o}C) quartz-fiber filters. Filter flow rates were individually adjusted with mass flowmeters (TSI, Model 4043) connected to a vacuum pump to obtain a range of filter loadings. A scanning mobility particle sizer (SMPS) consisting of an electrostatic classifier (TSI, Model 3080) and a condensation particle counter (CPC) (TSI, Model 3775) measured particle size distributions to estimate filter loading. Filters were stored at 0 ^{o}C after collection to minimize evaporation losses. Prior to analysis, particle-laden quartz-fiber filters were desiccated for more than 24 hours at 3.5% relative humidity to minimize water content. Evaporative losses during desiccation are expected to be small since samples are still at room temperature, and analysis starts at 80 ^{o}C. However, further analysis is needed to determine those losses. Portions of the inorganic filters were analyzed by IC for water-soluble ions (Chow and

Watson, 2017) and a punch (~0.5 cm^2) from the organic standards was analyzed by the standard TOA method for OC following the IMPROVE_A protocol.

Quantitative Analysis

Jimenez et al. (2003) outlines the EI-AMS approach to quantifying NH_4^+, NO_3^-, SO_4^{2-}, and OM. A similar approach is adapted for interpreting TOA-QMS spectra. The total number of molecules of a species *i*, M_i, entering the TOA-QMS is determined from an individual *m/z* signal as:

$$M_i = \frac{I_i}{X_i \times IE_i} \quad (1)$$

where I_i is the integrated signal (counts) due to species *i* at the specific *m/z* over the thermal desorption cycle; X_i is the fraction of the ions from species *i* that is detected at *m/z*; and IE_i is the ionization efficiency of species *i*, equaling the number of ions detected per molecule of the parent species. IE_i is species-specific and includes: electron ionization efficiency, transmission efficiency from the oven to the detector, the *m/z*-dependent transmission efficiency of the QMS, and the detection efficiency of the electron multiplier detector.

The mass density of the aerosol deposit for species *i*, C_i (μg cm^{-2}), that produces multiple ions at multiple *m/z* is:

$$C_i = \frac{10^6 MW_i}{IE_i \times A \times N_A} \sum I_{i,m/z} \quad (2)$$

where, 10^6 is the conversion factor for μg g^{-1}; MW_i is the molecular weight (g mol^{-1}) of species *i*; *A* is the filter punch area (~ 0.5 cm^2); N_A is Avogadro's number (molecules mol^{-1}); and the summation is over all fragment ions (i.e., *m/z* 1 to n) in the mass spectrum for species *i*.

The species-dependent IE_i and MW_i are not known for a complex ambient aerosol mixture, but Jimenez et al. (2003) demonstrate that IE_i/MW_i is distinct for inorganics, hydrocarbons, and oxygenated organics, meaning that relative *IEs* (*RIEs*) can be used to estimate species mass concentrations. The EI-AMS uses the *IE/MW* for NO_3^- as a reference for the *RIE*s of NH_4^+, SO_4^{2-}, and OM. Since the TOA-QMS system has an internal CO_2 calibration for every cycle (see Figure 2a), the CO_2 *IE/MW* can be used for this purpose. The IE_i/MW_i of any organic and inorganic molecule can be expressed as:

$$\frac{IE_i}{MW_i} = RIE_i \frac{IE_{CO_2}}{MW_{CO_2}} \quad (3)$$

and C_i can be re-written to include RIEs:

$$C_i = \frac{10^6 MW_{CO_2}}{RIE_i \times IE_{CO_2} \times A \times N_A} \sum I_{i,m/z} \quad (4)$$

where IE_{CO2} is the slope of the CO_2 calibration curve (i.e., summed *m/z* CO_2 signal divided by *m/z* signal of the calibration peak; see ionization efficiency in Figure 3) for the TOA-QMS. *RIEs* for NH_4^+, NO_3^-, and SO_4^{2-} are determined by first calculating the slope for individual species (Figure 4) and then calculating the *IE/MW* ratio to CO_2. For OM or OC, a similar procedure is employed by using data from many species that have been tested, thus calculating an average IE_{org}/MW_{org} for hydrocarbons and oxygenated organics. In this feasibility study, only OC was

estimated using the $C_2H_2O_4$ carbon content. OC would be measured separately in a TOA system, so the purpose served here was to determine how well the EI-QMS might reproduce that value.

The partial mass spectrum of species *i*, $I_{i,m/z}$, showing the ion contribution from species *i* at each *m/z*, is estimated based on a fragmentation table similar to that of the EI-AMS described by Allan et al. (2004). There are important differences between the TOA-QMS and EI-AMS: 1) the particle collection media are quartz-fiber filters in TOA-QMS and a metal cup in EI-AMS; 2) it takes the TOA several seconds to heat the sample to a specified temperature (e.g., 80º C to 580 ºC), while the EI-AMS vaporizer is maintained at a constant temperature (~600 ºC) which flash vaporizes non-refractory PM in < 1 ms (Canagaratna et al., 2007); 3) the TOA vaporizes PM in a pressurized carrier gas (~1.7 $\times 10^5$ Pa), while the EI-AMS vaporizes PM under vacuum (~10^{-5} Pa); 4) the TOA-QMS ionizes the vapors after longer transport time from the TOA to the QMS, while the EI-AMS ionizes the vapors right after vaporization; 5) the TOA-QMS uses He as the carrier gas and EI-AMS typically uses air as the carrier gas; and 6) the TOA-QMS heats samples up to 840 ^{o}C, higher than that in EI-AMS (~600 ^{o}C). Therefore, the TOA-QMS is able to analyze data over a more stable and controlled environment, with less interference from external ambient factors. These differences result in similar *m/z* patterns, but different *m/z* signal magnitudes between the TOA-QMS and EI-AMS. Therefore, while qualitatively similar, the EI-AMS fragmentation tables are not directly applicable to the TOA-QMS. Development of fragmentation tables for the TOA-QMS is the primary focus of this work.

Figure-4 shows the relationship between the TOA-QMS response and the independent IC and TOA measurements. The response curves indicate both reproducibility and linearity for the calibration compounds.

Fragmentation Corrections

NH_4NO_3, $(NH_4)_2SO_4$, $C_2H_2O_4$, and CO_2 mass spectra from the TOA-QMS and EI-AMS are compared in Figure 5, demonstrating the different relative *m/z* signal intensities. The NH_4NO_3 spectrum (Figure 5a) shows ion peaks at *m/z* 14 (N^+), 15 (NH^+), 16 (NH_2^+), 17 (NH_3^+), 18 (NH_4^+), 30 (NO^+), and 46 (NO_2^+). The TOA-QMS also shows CO_2 interference at *m/z* 44. The $(NH_4)_2SO_4$ spectrum shows signals at *m/z* 14 (N^+), 15 (NH^+), 16 (NH_2^+), 17 (NH_3^+), 18 (NH_4^+), 32 (S^+), 48 (SO^+), and 64 (SO_2^+). EI-AMS signals at *m/z* 80 (SO_3^+), 81 (HSO_3^+), and 98 ($H_2SO_4^+$) in Figure 5b were not detected by the TOA-QMS. The TOA-QMS spectrum for $C_2H_2O_4$ (Figure 5c) shows major signals at *m/z* 29, 44, 45, and 46, while the EI-AMS shows major $C_2H_2O_4$ signals at *m/z* 17, 27, and 43. Similar mass spectra for CO_2 with ion peaks at *m/z* 28 and 44 are shown in Figure 5d. These differences in spectra are likely due to inherent difference in the two systems as discussed in the previous section.

NH_4^+, NO_3^-, and SO_4^{2-} mass concentrations were estimated following the format described by Allan et. al. (2004) and are presented in the following text, with additional information in Table 1. Most of the *m/z* signals have contributions from more than one of the major species. NH_4^+, NO_3^-, and SO_4^{2-} become positively charged in the election impact ionization process and are therefore denoted as NH_4^+, NO_3^+ and SO_4^+. In the following equations, *m/z* signals labeled with a subscript indicate contributions from the major species to

each *m/z* signal (not the entire *m/z* signal). The subscript *sum* denotes the total *m/z* signal for the species (a sum of all contributing ions or *m/z* signals), and the subscript *sig* represents the total *m/z* signal from all compounds for the specified *m/z*. The subscript *organic* is used to denote OC contributions. While simple calibration and measurement of the major species could be performed using just a few of the ions, this work attempts to account for all contributing fragments (*m/z* signals) to the inorganic species, so that the remainder of the *m/z* signals can be attributed to OC. This would assume that there are no interferences from other compounds, most of which (e.g., EC and geological minerals) are not expected to decompose in the inert atmosphere. The remaining *m/z* signal was related to equivalent OC using TOA-FID analysis of $C_2H_2O_4$ standards.

Deconvolution of the ambient mass spectrum begins with removing interferences from the NH_4^+ spectrum. The total NH_4^+ signal ($NH_4^+{}_{Sum}$) is represented as follows:

$$NH_4^+{}_{Sum} = m/z\ 14_{(NH_4^+)} + m/z\ 15_{(NH_4^+)} + m/z\ 16_{sig} + m/z\ 17_{(NH_4^+)} \quad (5)$$

where $m/z\ 14_{(NH_4^+)}$, $m/z\ 15_{(NH_4^+)}$, and $m/z\ 17_{(NH_4^+)}$ represent the NH_4^+ contributions to *m/z* 14, 15, and 17, respectively, while $m/z\ 16_{sig}$ represents the total signal of *m/z* 16 as it is considered to come entirely from NH_4^+. Interferences from other compound fragments for *m/z* 14, 15, and 17 are taken into account as follows:

$$m/z\ 14_{(NH_4^+)} = m/z\ 14_{sig} - 0.0178 \times m/z\ 30_{sig} - 0.17818 \times m/z\ 46_{sig} \quad (6)$$

$$m/z\ 15_{(NH_4^+)} = 0.0802 \times m/z\ 16_{sig} \quad (7)$$

$$m/z\ 17_{(NH_4^+)} = m/z\ 17_{sig} - 0.2122 \times m/z\ 18_{(OH^+)} \quad (8)$$

where $m/z\ 14_{sig}$ (Eq. 6) is the total *m/z* 14 signal in the spectrum; the ratios, 0.0178 and 0.17818, represent the fractions of *m/z* 14 generated from the dissociation of NO^+ (*m/z* 30) and NO_2^+ (*m/z* 46), respectively, for pure NO_3^+ (see Table 1), while the remainder of the *m/z* 14 signal represents the dissociation of NH_4^+ (*m/z 18)* to N^+ (*m/z* 14). The use of these ratios for approximating the contributions from *m/z* 30 and 46 assumes that organic fragment interferences are minimal (Allan et. at., 2004). The *m/z* 15 signal (Eq. 7) results from the fragmentation of NH_2^+ (*m/z* 16) into NH^+ (*m/z* 15). Therefore, the NH_4^+ contribution to the *m/z* 15 signal is found by the ratio of *m/z* 15 to *m/z* 16. Since *m/z* 16 is assumed to be completely from the fragmentation of NH_4^+ into NH_2^+, it requires no adjustment for interferences. The *m/z* 17 signal (Eq. 8) results from both NH_4^+ and OH^+, a fragment of H_2O, which is removed using a *m/z* 17 to *m/z* 18 ratio (i.e., 0.2122) from the H_2O spectrum (National Institute of Standards and Technology, NIST, 2014). Elevated H_2O concentrations may introduce higher uncertainties, but this should be minimal as samples were desiccated and dried in the analyzer at 80°C to reduce H_2O content.

Major NO_3^+ fragments are found at *m/z* 30 and 46 signals, constituting 72.75 ± 12.62% of the total NO_3^+ *m/z* signal. The total NO_3^+ *m/z* signal, denoted as $NO_{3\ sum}^+$, is determined as follows:

$$NO_{3\ sum}^+ = m/z\ 14_{(NO_3^+)} + m/z\ 30_{(NO_3^+)} + m/z\ 31_{(NO_3^+)} + m/z\ 32_{(NO_3^+)} + m/z\ 44_{(NO_3^+)} + m/z\ 46_{sig} + m/z\ 47_{(NO_3^+)} + m/z\ 48_{(NO_3^+)} \quad (9)$$

where $m/z\ 14_{(NO_3^+)}$, $m/z\ 30_{(NO_3^+)}$, $m/z\ 31_{(NO_3^+)}$, $m/z\ 32_{(NO_3^+)}$, $m/z\ 44_{(NO_3^+)}$, $m/z\ 47_{(NO_3^+)}$, and $m/z\ 48_{(NO_3^+)}$, represent the NO_3^+ contribution to *m/z* 14, 30, 31, 32, 44, 47, and 48, respectively. The entire *m/z* 46 signal is assumed to be due to NO_3^+ and therefore denoted as $m/z\ 46_{sig}$. The NO_3^+ contribution to the remaining *m/z* signals are determined similar to those for NH_4^+, using the following equations:

$$m/z\ 14_{(NO_3^+)} = 0.0178 \times m/z\ 30_{sig} + 0.17818 \times m/z\ 46_{sig} \quad (10)$$

$$m/z\ 30_{(NO_3^+)} = m/z\ 30_{sig} - 0.022 \times m/z\ 29_{sig} \quad (11)$$

$$m/z\ 31_{(NO_3^+)} = 0.00405 \times m/z\ 30_{sig} \quad (12)$$

$$m/z\ 32_{(NO_3^+)} = 0.002 \times m/z\ 30_{sig} \quad (13)$$

$$m/z\ 44_{(NO_3^+)} = 2 \times m/z\ 46_{sig} + 0.2 \times m/z\ 30_{sig} \quad (14)$$

$$m/z\ 47_{(NO_3^+)} = 0.00443 \times m/z46_{sig} \quad (15)$$

$$m/z\ 48_{(NO_3^+)} = 0.004 \times m/z\ 46_{sig} \quad (16)$$

The NO_3^+ fraction of *m/z* 14 is determined from the *m/z* 14 to *m/z* 30 and *m/z* 14 to *m/z* 46 ratios (i.e., 0.0178 and 0.17818) resulting from the dissociation of NO^+ and NO_2^+, respectively (Eq. 10). A small contribution from organic fragment containing ^{13}C affects the *m/z* 30 signal (Eq. 11) and is approximated using a fraction of the *m/z* 29 signal, based upon the *m/z* 30 to *m/z* 29 ratio predicted using the International Union of Pure and Applied Chemistry (IUPAC) spectral information (Allan et al.,2004). The NO_3^+ portions of *m/z* 31 and *m/z* 32 are based on pure NO_3^+

ratios to *m/z* 30. Separating nitrous oxide (N_2O^+) from OC at *m/z* 44 (i.e., *m/z* 44 could represent CO_2, vinyl alcohol [CH_2CHOH], etc.) is accomplished by finding the fraction of the signal at *m/z* 44 in relation to *m/z* 46 and *m/z* 30 signals (Eq. 14). The *m/z* 46 signal is assumed to be completely from the fragmentation of NO_3^+ into NO_2^+, and signals at *m/z* 47 and *m/z* 48 signals are fractions of the parent signal at *m/z* 46 signal based on IUPAC isotopic abundances (Eqs. 15 and 16). Similar to the EI-AMS, and because only the *m/z* 30 and 46 signal contribution to the spectrum were used to derive the NO_3^+ RIE, an adjustment factor that includes the omitted fragments is necessary to correctly estimate the nitrate mass concentration (Hogrefe et al., 2004). An adjustment factor of 1.36 was used for TOA-QMS.

TOA-QMS derived SO_4^{2-} dominates signals at *m/z* 18, 48, and 64, which accounts for 77.28 ± 14.48% of the total *m/z* signal for this species. The total SO_4^{2-} signal, ${SO_4^{2-}}_{sum}$, is represented by the partial contribution from *m/z* 18, 48, and 64 signals:

$${SO_4^{2-}}_{sum} = m/z\ 18_{(SO_4^{2-})} + m/z\ 48_{(SO_4^{2-})} + m/z\ 64_{(SO_4^{2-})} \quad (17)$$

where $m/z\ 18_{(SO_4^{2-})}$, $m/z\ 48_{(SO_4^{2-})}$, and $m/z\ 64_{(SO_4^{2-})}$ represent the SO_4^{2-} contribution to *m/z* 18, 48, and 64, respectively. Identities of the sulfate ion fragments are listed in Table 1. Contributions to *m/z* 18, 48, and 64 signals are illustrated as follows:

$$m/z\ 18_{(SO_4^{2-})} = 0.49 \times m/z\ 48_{sig} + 0.268 \times m/z\ 64_{sig} \quad (18)$$

$$m/z\ 48_{(SO_4^{2-})} = m/z\ 48_{sig} - m/z\ 48_{(NO_3^+)} - m/z\ 62_{sig} \quad (19)$$

$$m/z\ 64_{(SO_4^{2-})} = m/z\ 64_{sig} - m/z\ 64_{organic} \quad (20)$$

The SO_4^{2-} signal at *m/z* 18 signal (Eq. 18) was calculated using the signal ratios between *m/z* 18 signal to *m/z* 48 signal and *m/z* 18 signal to *m/z* 64 signal, i.e., 0.49 and 0.268, respectively. The SO_4^{2-} signal at *m/z* 48 (Eq. 19) is represented by the signal at *m/z* 48 minus the interference signals from NO_3^+ at *m/z* 48 and an organic contribution estimated as the *m/z* 62 signal. The SO_4^{2-} *m/z* signal at *m/z* 64 (Eq. 20) is represented by the signal at *m/z* 64 minus a fraction of the *m/z* 50 signal and the *m/z* 78 signal as:

$$m/z\ 64_{organic} = 0.5 \times m/z\ 50_{sig} + 0.5 \times m/z\ 78_{sig} \quad (21)$$

While only an approximation of the organics contribution to *m/z* 64 signal, the signals at *m/z* 50 and 78 are used since they represent the addition and subtraction of a CH_2 group from a hydrocarbon chain (Allan et al. 2004). Figure 6 shows the process for separating OC from the inorganic species. The OC total *m/z* signal is calculated by subtracting the sum of the calculated *m/z* signals of the major inorganic species from the spectrum total *m/z* signal. $C_2H_2O_4$ was used to relate the OC total *m/z* signal to OC mass loading by plotting OC concentration from the $C_2H_2O_4$ loaded filters using the TOA-FID against the TOA-QMS summed *m/z* signal of the same C□H□O□ loaded filter. This serves as a calibration curve to estimate total OC in ambient samples (see Figure 4d). OM can be estimated by relating the carbon in $C_2H_2O_4$ to its molecular weight; however, OM is not reported here as $C_2H_2O_4$ is highly oxygenated, while OM/OC multiplier varies by location and time (Turpin and Lim, 2001). Further investigation of the spectral data for various organic compounds may offer differentiation between different levels of oxygenated organics, providing the means to better approximate OM and the OM/OC multiplier.

The method detection limit (MDL) for each species is determined by applying the fragmentation table to blank quartz-fiber filters or, in case no signal is detected by the EI-QMS, the y-intercept of the calibration curve. MDLs for NH_4^+, NO_3^-, SO_4^{2-}, and organic carbon equivalent (OCe) species were 1.59, 0.07, 0.96, and 4.22 $\mu g \cdot cm^{-2}$, respectively. In comparison, MDLs for ions by IC and for OC by TOA are 0.10 and 0.43 $ug \cdot cm^{-2}$, respectively. The method may not be as applicable as IC and TOA for samples from pristine environments, but these MDLs are adequate for polluted cities. Different blank filter sets result in slightly different MDLs, and all blank filters (N=100) were averaged for the MDLs reported in this study.

The higher MDLs of the current method may be a result of several aspects of the instrument: 1) air intrusion; and 2). cold spots that may cause condensation of desorbed PM from the quartz-fiber filter. Ambient air may enter the TOA-QMS through the entry port, and further reducing this would reduce oxidation of the ionization filament. While a reduction of cold spots was attempted, some may still be present, causing condensation and further affecting MDLs. More specific heating of the transfer lines, which is possible with a later version of the TOA, could minimize condensation.

A MatLab (MATLAB R2014a, The MathWorks Inc., Natick, MA) program processed three-dimensional (*m/z* spectra vs. time) raw data from the QMS by integrating ion currents at each temperature level using the Riemann (1868) sum method. A baseline was determined at each temperature step for each *m/z* spectrum and subtracted from the sample signal. Integrated *m/z* signal is normalized using the *m/z* signal from a CO_2 calibration standard injected at the end of each run. This allows comparison of data from run to run, accounting for slight changes in the

system. The *m/z* signals obtained from TOA-QMS analysis of blank filters are subtracted from sample mass spectral data and the remaining *m/z* signals are then de-convoluted into NH_4^+, NO_3^-, SO_4^{2-}, and OC fractions.

The current software removes interferences from ions associated with the ion of interest automatically. The software allows the user to modify and select the fragmentation tables, detection limits, correction factors, and baseline as needed and depending on the properties of the instrument being used. Future software development would include a user interface that allows rapid inspection of the spectra and performance parameters.

Real-World Sample Analyses

Quartz-fiber filter sample remnants were selected from the refrigerated archive to represent a variety of PM compositions, including: 1) 58 samples with 16 replicates from the Fresno Supersite (Watson et al., 2000); 2) three Fresno samples each from winter, spring, and summer with five replicates, (15 total); and 3) 11 samples from near Baltimore, MD (Chen et al., 2002). These samples had been previously analyzed for ions by IC and OC by TOA. Fresno samples contained high NO_3^- concentrations, while Baltimore samples contained high SO_4^{2-} concentrations.

Figure-7 compares the mass loadings of inorganic ions and OC by TOA-QMS with those by IC and TOA analyses. Although reasonable linearity and high correlations were observed for Fresno ions and OC samples (R^2 = 0.88 to 0.96), and for Baltimore NH_4^+, SO_4^{2-}, and OC samples (R^2 = 0.94 to 0.99), no linearity was found for Baltimore NO_3^- samples, likely due to the very

low NO_3^- levels. Compared to IC analysis of these ambient samples, the TOA-QMS calibrated with the pure compound samples underestimates NO_3^- by 24% but overestimates SO_4^2 by 29%. These deviations are similar to the ±26% reported by the EI-AMS for inorganic measurements when compared with a collocated Particle-into-Liquid Sampler (PILS) (Canagaratna et al., 2007). Discrepancies are possibly due to interference between organic and inorganic signals, or to the formation of different ions as fragmentation occurs. Water-soluble SO_4^{2-} measured by IC excludes insoluble organosulfates (e.g., $ROSO_3$) and other insoluble salts (e.g., $BaSO_4$, $PbSO_4$, Ag_2SO_4 and $SrSO_4$) (Hawkins et al., 2010), but these are not expected to be major components found in the atmosphere. The good agreement for NH_4^+ (slopes of 0.96 for Fresno and 0.85 for Baltimore) indicates that the NO_3^- deficit is related to the SO_4^{2-} surplus, suggesting that a better calibration might be achieved using mixed-salt standards. It also appears from Figure 7 that the lower NO_3^- and SO_4^{2-} concentrations are closer to the 1:1 line than the higher concentrations, indicating that separate calibration curves might be needed for the higher concentrations. The $C_2H_2O_4$ calibration appears to account well for the OC measured by TOA, which could be a quality control on the TOA when the method is applied in a parallel-stream mode, or possibly even a substitute for the FID.

Figure-8 shows that average TOA-QMS derived concentrations can be comparable to those of routine measurements using IC for the 58 Fresno samples. Correction factors (CFs) are sometimes used with EI-AMS measured concentrations to match the concentrations with more established methods (Drewnick et al., 2003; Hogrefe et al., 2004; Jimenez et al., 2003). Using the average ratios of (TOA-QMS)/IC, the CFs are 1.36 for NO_3^- and 0.80 for SO_4^{2-}. After applying

these CFs, Figure 9 shows 1:1 comparisons between TOA-QMS and IC measurements with close to unity slopes and high correlations (0.91-0.96).

Figure-10 presents a time series of $PM_{2.5}$ compositions at Fresno corresponding to the 58 samples taken over the period of 12/15/2000 – 2/3/2001 (Chow et al., 2008). Concentrations increased from 12/27/2000 to 1/7/2001 during a prolonged high pressure system between storms. $PM_{2.5}$ NO_3^- and OC concentrations during the haze period were elevated, confirming that NO_3^- is a large $PM_{2.5}$ component, as is well-known for winter in central California (Reynolds et al., 2012). Large diurnal variations are also found with elevated NO_3^- and OC during the 16:00-24:00 local standard time.

Summary, Conclusions, and Future Work

This feasibility study demonstrates the possibility of adapting the TOA analysis to obtain major ions, as well as organic carbon from quartz-fiber filter samples, by analyzing the thermally-liberated species with an EI-QMS. It is found that spectra similar to those obtained by the EI-AMS can be obtained, but that the ratios of the *m/z* signals differ and must be re-measured using laboratory generated standards. Linear relationships are found between QMS signals and prepared standards of NH_4^+, NO_3^-, and SO_4^{2-}. For ambient samples, however, positive deviations are found for SO_4^{2-}, compensated by negative deviations for NO_3^-, at higher concentrations. This indicates the possible need to use mixed-compound standards for calibration or separate calibration curves for low and high ion concentrations. The sum of the QMS signals across all *m/z* after removal of the NH_4^+, NO_3^-, and SO_4^{2-} signals was highly correlated with the carbon

content of $C_2H_2O_4$ standards. For ambient samples, the OC derived from the TOA-QMS method was nearly the same as the OC derived from the standard IMPROVE_A TOA method.

This setup is a practical possibility for the newly-designed DRI Model 2015 TOA (McGee Scientific, Berkeley, CA). This instrument also allows for simultaneous determination of multi-wavelength light absorption and separation of brown carbon from black carbon (Chen et al., 2015; Chow et al., 2015b), as well as providing more precise sample heating that can better bracket the decomposition temperatures of different compounds found in suspended particles (MacKenzie, 1970).

Although the feasibility for this approach is evident, there are several issues that need to be resolved in further testing before attempting to adapt TOA to multi-species measurements:

- More experiments are needed to explain why the standardization with pure compounds provided different TOA-QMS responses in real-world samples. This can be explored by using mixtures with different proportions of nitrate and sulfate salts on standards generated by the aerosolization process as described here. Calibrations with more organic compounds are needed to drive more representative RIEs for organic aerosol fractions.

- The EI-QMS portion of the EI-AMS might be a better choice than the generic EI-QMS used for these tests, as this appears to be more optimized for ambient aerosols. Daellenback et al. (2016) and Bozetti et al (2017) have demonstrated the offline use of an AMS by nebulizing water-soluble filter extracts, finding adequate detection limits and good reproducibility. There are also rapid advances in miniature mass spectrometers (Blakeman et al., 2017; Snyder et al.,

2016) that may eventually replace the more standard, general-purpose laboratory units. Such a Mini-MS has been demonstrated in a field unit for thermal desorption OC measurements (Cropper, 2016).

- Mass spectra deconvolution methods are continually improving, much of it motivated by the various AMS versions that are being deployed in source characterization and ambient studies. More advanced approaches that better remove interferences among the aerosol mixture can be incorporated into the TOA-QMS software.

- The parallel sample approach can be implemented in the new Model 2015 TOA to add value to the measurements already being acquired in long-term speciation networks with minimal added analysis cost. Even when used with multiple filters accompanied by IC analysis, the single analysis approach would be a useful adjunct.

Acknowledgements

This research was partially supported by National Science Foundation Grant Nos. 1214163 and 1464501, and the National Park Service IMPROVE Carbon Analysis Contract (C2350000894). Drs. Glenn Miller of the University of Nevada, Reno, Lung Wen Anthony Chen of the University of Nevada, Las Vegas, and Jerome Robles of the Government of British Columbia, Canada, provided useful suggestions for the experiments and their description.

References

Allan, J.D., et al. 2004. A generalised method for the extraction of chemically resolved mass spectra from aerodyne aerosol mass spectrometer data. *J. Aerosol Sci.*, 35:909-922.

Blakeman, K.H., Cavanaugh, C.A., Gilliland, W.M. and Ramsey, J.M. 2017. High pressure mass spectrometry of volatile organic compounds with ambient air buffer gas. *Rapid Communications in Mass Spectrometry*, 31:27-32. 10.1002/rcm.7766.

Bozzetti, C., et al. 2017. Argon offline-AMS source apportionment of organic aerosol over yearly cycles for an urban, rural, and marine site in northern Europe. *Atmos. Chem. Phys*, 17:117-141. 10.5194/acp-17-117-2017.

Canagaratna, M.R., et al. 2007. Chemical and microphysical characterization of ambient aerosols with the aerodyne aerosol mass spectrometer. *Mass Spectrometry Reviews*, 26:185-222.

Chen, L.-W.A., Doddridge, B.G., Dickerson, R.R., Chow, J.C. and Henry, R.C. 2002. Origins of fine aerosol mass in the Baltimore-Washington corridor: Implications from observation, factor analysis, and ensemble air parcel back trajectories. *Atmos. Environ.*, 36:4541-4554.

Chen, L.-W.A., Chow, J.C., Watson, J.G. and Schichtel, B.A. 2012. Consistency of long-term elemental carbon trends from thermal and optical measurements in the IMPROVE network. *Atmos. Meas. Tech.*, 5:2329-2338.

Chen, L.-W.A., Chow, J.C., Wang, X.L., Robles, J.A., Sumlin, B.J., Lowenthal, D.H., Zimmermann, R. and Watson, J.G. 2015. Multi-wavelength optical measurement to enhance thermal/optical analysis for carbonaceous aerosol. *Atmos. Meas. Tech.*, 8:451-461.

Chow, J.C., Watson, J.G., Bowen, J.L., Frazier, C.A., Gertler, A.W., Fung, K.K., Landis, D. and Ashbaugh, L.L. 1993a. A sampling system for reactive species in the western United States, Winegar, E.D. and Keith, L.H. (Eds.), *Sampling and Analysis of Airborne Pollutants,* Ann Arbor, MI: Lewis Publishers. 209-228.

Chow, J.C., Watson, J.G., Pritchett, L.C., Pierson, W.R., Frazier, C.A. and Purcell, R.G. 1993b. The DRI Thermal/Optical Reflectance carbon analysis system: Description, evaluation and applications in U.S. air quality studies. *Atmos. Environ.*, 27A:1185-1201.

Chow, J.C. and Watson, J.G. 1999. Ion chromatography in elemental analysis of airborne particles, Landsberger, S. and Creatchman, M. (Eds.), *Elemental Analysis of Airborne Particles, Vol. 1,* Amsterdam: Gordon and Breach Science. 97-137.

Chow, J.C., Watson, J.G., Chen, L.-W.A., Chang, M.-C.O., Robinson, N.F., Trimble, D.L. and Kohl, S.D. 2007. The IMPROVE_A temperature protocol for thermal/optical carbon analysis: Maintaining consistency with a long-term database. *J. Air Waste Manage. Assoc.*, 57:1014-1023.

Chow, J.C., Watson, J.G., Lowenthal, D.H., Park, K., Doraiswamy, P., Bowers, K. and Bode, R. 2008. Continuous and filter-based measurements of PM2.5 nitrate and sulfate at the Fresno Supersite. *Environ. Mon. Assess*, 144:179-189.

Chow, J.C., Watson, J.G., Robles, J., Wang, X.L., Chen, L.-W.A., Trimble, D.L., Kohl, S.D., Tropp, R.J. and Fung, K.K. 2011. Quality assurance and quality control for thermal/optical analysis of aerosol samples for organic and elemental carbon. *Analytical and Bioanalytical Chemistry*, 401:3141-3152. DOI 10.1007/s00216-011-5103-3.

Chow, J.C. and Watson, J.G. 2013. Chemical analyses of particle filter deposits, Ruzer, L. and Harley, N.H. (Eds.), *Aerosols Handbook : Measurement, Dosimetry, and Health Effects,* 2 ed. New York, NY: CRC Press/Taylor & Francis. 179-204.

Chow, J.C., Lowenthal, D.H., Chen, L.-W.A., Wang, X.L. and Watson, J.G. 2015a. Mass reconstruction methods for $PM_{2.5}$: A review. *Air Qual. Atmos. Health*, 8:243-263.

Chow, J.C., et al. 2015b. Optical calibration and equivalence of a multiwavelength thermal/optical carbon analyzer. *Aerosol Air Qual. Res.*, 15:1145-1159. doi:10.4209/aaqr.2015.02.0106.

Chow, J.C. and Watson, J.G. 2017. Enhanced ion chromatographic speciation of water-soluble PM2.5 to improve aerosol source apportionment. *Aerosol Science and Engineering*, 1:7-24. doi:10.1007/s41810-017-0002-4.

Cropper, P.M. 2016. Determination of fine particulate matter composition and development of the organic aerosol monitor. PhD dissertation, Brigham Young University, Provo, UT. http://scholarsarchive.byu.edu/cgi/viewcontent.cgi?article=6667&context=etd (Accessed July 31, 2017)

Daellenbach, K.R., et al. 2016. Characterization and source apportionment of organic aerosol using offline aerosol mass spectrometry. *Atmos. Meas. Tech.*, 9:23-39. 10.5194/amt-9-23-2016.

Diab, J., et al. 2015. Hyphenation of a EC/OC thermal-optical carbon analyzer to photo ionization time-of-flight mass spectrometry: A new off-line aerosol mass spectrometric approach for characterization of primary and secondary particulate matter. *Atmos. Meas. Tech.*, 8:3337-3353.

Drewnick, F., Schwab, J.J., Hogrefe, O., Peters, S., Husain, L., Diamond, D., Weber, R. and Demerjian, K.L. 2003. Intercomparison and evaluation of four semi-continuous PM2.5 sulfate instruments. *Atmos. Environ.*, 37:3335-3350.

Fiore, A.M., Naik, V. and Leibensperger, E.M. 2015. Critical review: Air quality and climate connections. *J. Air Waste Manage. Assoc.*, 65:645-685.

Grabowsky, J., Streibel, T., Sklorz, M., Chow, J.C., Mamakos, A. and Zimmermann, R. 2011. Hyphenation of a carbon analyzer to photo-ionization mass spectrometry to unravel the organic composition of particulate matter on a molecular level. *Analytical and Bioanalytical Chemistry*, 401:3153-3164.

Grahame, T.J., Klemm, R.J. and Schlesinger, R.B. 2014. Public health and components of particulate matter: The changing assessment of black carbon: Critical Review. *J. Air Waste Manage. Assoc.*, 64:620-660.

Hawkins, L.N., Russell, L.M., Covert, D.S., Quinn, P.K. and Bates, T.S. 2010. Carboxylic acids, sulfates, and organosulfates in processed continental organic aerosol over the southeast Pacific Ocean during VOCALS-REx 2008. *J. Geophys. Res. Atmos.*, 115, D13201, doi:10.1029/2009jd013276

Hidy, G.M., Mueller, P.K., Altshuler, S.L., Chow, J.C. and Watson, J.G. 2017. Critical review: Air quality measurements—From rubber bands to tapping the rainbow. *J. Air Waste Manage. Assoc.*, 67:637-668.

Hogrefe, O., Drewnick, F., Lala, G.G., Schwab, J.J. and Demerjian, K.L. 2004. Development, operation and applications of an aerosol generation, calibration and research facility. *Aerosol Sci. Technol.*, 38:196-214.

Jayne, J.T., Leard, D.L., Zhang, X., Davidovits, P., Smith, K.A., Kolb, C.E. and Worsnop, D.R. 2000. Development of an aerosol mass spectrometer for size and composition analysis of submicron particles. *Aerosol Sci. Technol.*, 33:49-70.

Jimenez, J.L., et al. 2003. Ambient aerosol sampling using the Aerodyne aerosol mass spectrometer. *Journal of Geophysical Research*, 108:SOS13-11-SOS13-13. doi:10.1029/2001JD001213.

Kerminen, V.M., Ojanen, C., Pakkanen, T., Hillamo, R., Aurela, M. and Merilainen, J. 2000. Low-molecular-weight dicarboxylic acids in an urban and rural atmosphere. *J. Aerosol Sci.*, 31:349-362.

Lozano, R., et al. 2012. Global and regional mortality from 235 causes of death for 20 age groups in 1990 and 2010: A systematic analysis for the Global Burden of Disease Study 2010. *Lancet*, 380:2095-2128.

Malm WC, Sisler JF, Huffman D, Eldred RA, Cahill TA (1994) Spatial and seasonal trends in particle concentration and optical extinction in the United States. J Geophys Res 99:1347-1370.

MacKenzie, R.C. 1970. *Differential Thermal Analysis Vol. 1: Fundamental Aspects*. New York, NY: Academic Press.

Murphy, D.M., Chow, J.C., Leibensperger, E.M., Malm, W.C., Pitchford, M.L., Schichtel, B.A., Watson, J.G. and White, W.H. 2011. Decreases in elemental carbon and fine particle mass in the United States. *Atmos. Chem. Phys*, 11:4679-4686.

NIST 2014. NIST/EPA/NIH mass spectral library (NIST 14) and NIST Mass Spectral Search Program (Version 2.2). National Institute of Standards and Technology, Gaithersberg, MD. https://www.nist.gov/document-3168 (Accessed July 31, 2017)

Pope, C.A. and Dockery, D.W. 2006. Critical Review: Health effects of fine particulate air pollution: Lines that connect. *J. Air Waste Manage. Assoc.*, 56:709-742.

Reynolds, S., et al. 2012. Synthesis of CCOS and CRPAQS study findings. San Joaquin Valley Unified Air Pollution Control District, Fresno, CA. https://www.researchgate.net/publication/316170523_Synthesis_of_CCOS_and_CRPAQS_study_findings (Accessed July 31, 2017)

Riemann, B. 1868. Über der Begriff eines bestimmten Integrals und den Umfang seiner Gültigkeit: . *Abhandlungen der Königlichen Gesellschaft der Wissenschaften zu Göttingen*, 13:87-132.

Riggio, G.M. 2015. Development and application of thermal/optical- quadrupole TOA-QMS mass spectrometry for quantitative analysis of major particulate matter constituents, M.S. Thesis. University of Nevada, Reno, Reno, NV.

Snyder, D.T., Pulliam, C.J., Ouyang, Z. and Cooks, R.G. 2016. Miniature and fieldable mass spectrometers: Recent advances. *Anal. Chem.*, 88:2-29. 10.1021/acs.analchem.5b03070.

Solomon, P.A., Crumpler, D., Flanagan, J.B., Jayanty, R.K.M., Rickman, E.E. and McDade, C.E. 2014. US National $PM_{2.5}$ Chemical Speciation Monitoring Networks-CSN and IMPROVE: Description of networks. *J. Air Waste Manage. Assoc.*, 64:1410-1438.

Turpin, B.J. and Lim, H.J. 2001. Species contributions to $PM_{2.5}$ mass concentrations: Revisiting common assumptions for estimating organic mass. *Aerosol Sci. Technol.*, 35:602-610.

Watson, J.G., Chow, J.C. and Frazier, C.A. 1999. X-ray fluorescence analysis of ambient air samples, Landsberger, S. and Creatchman, M. (Eds.), *Elemental Analysis of Airborne Particles, Vol. 1,* Amsterdam, The Netherlands: Gordon and Breach Science. 67-96.

Watson, J.G., Chow, J.C., Bowen, J.L., Lowenthal, D.H., Hering, S.V., Ouchida, P. and Oslund, W. 2000. Air quality measurements from the Fresno Supersite. *J. Air Waste Manage. Assoc.*, 50:1321-1334.

Watson, J.G. 2002. Visibility: Science and regulation - 2002 Critical Review. *J. Air Waste Manage. Assoc.*, 52:628-713.

Watson, J.G., Chow, J.C., Engling, G., Chen, L.-W.A. and Wang, X.L. 2016. Source apportionment: Principles and methods, Harrison, R.M. (Ed.) *Airborne Particulate Matter: Sources, Atmospheric Processes and Health,* London, UK: Royal Society of Chemistry. 72-125.

Watson, J.G., Tropp, R.J., Kohl, S.D., Wang, X.L. and Chow, J.C. 2017. Filter processing and gravimetric analysis for suspended particulate matter samples. *Aerosol Science and Engineering*, 1:193-205.

Yang, F., Chen, H., Wang, X.N., Yang, X., Du, J.F. and Chen, J.M. 2009. Single particle mass spectrometry of oxalic acid in ambient aerosols in Shanghai: Mixing state and formation mechanism. *Atmos. Environ.*, 43:3876-3882.

Figure 1. Schematic of the TOA-QMS system for PM $_{2.5}$ organic carbon and inorganic species measurement.

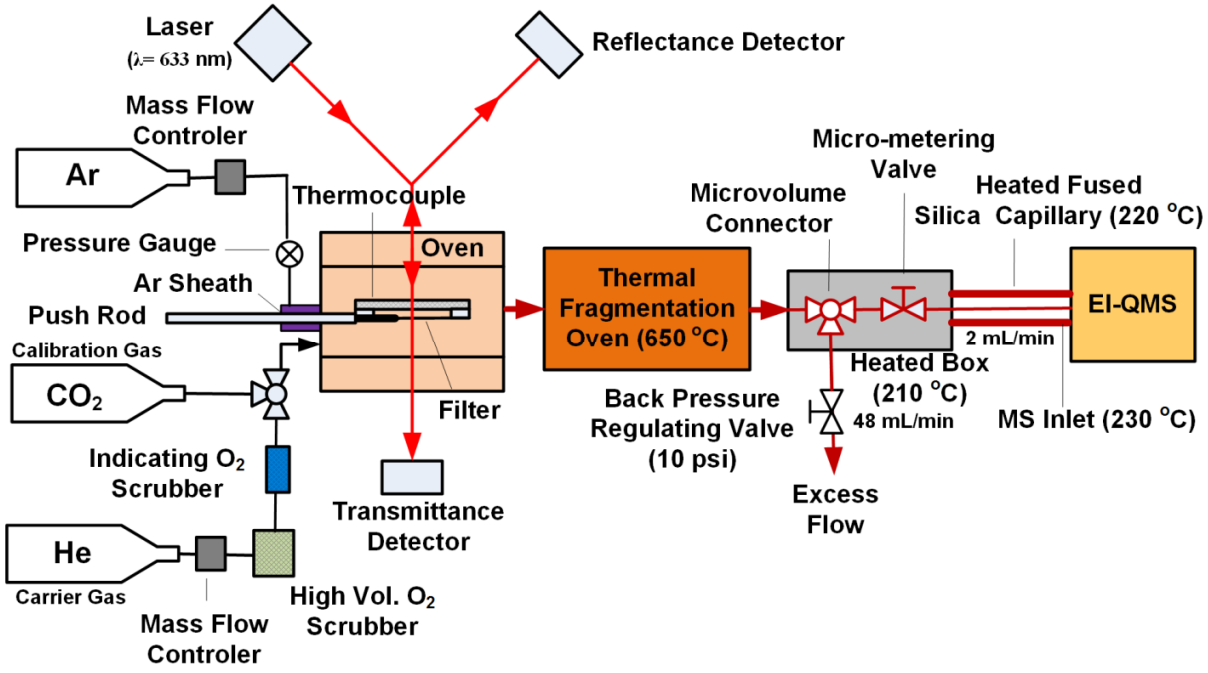

Figure 2. (a) Thermogram from burning of a birch log collected on a quartz-fiber filter comparing the IMPROVE_A temperature protocol with the simplified protocol used with the TOA-QMS; and (b) TOA-QMS spectrum obtained for the 580 ^{o}C portion from *m/z* 10 to 250, which constitutes most of the evolved gases. Major features are noted at *m/z* 27, 39, 44, 91, and 115.

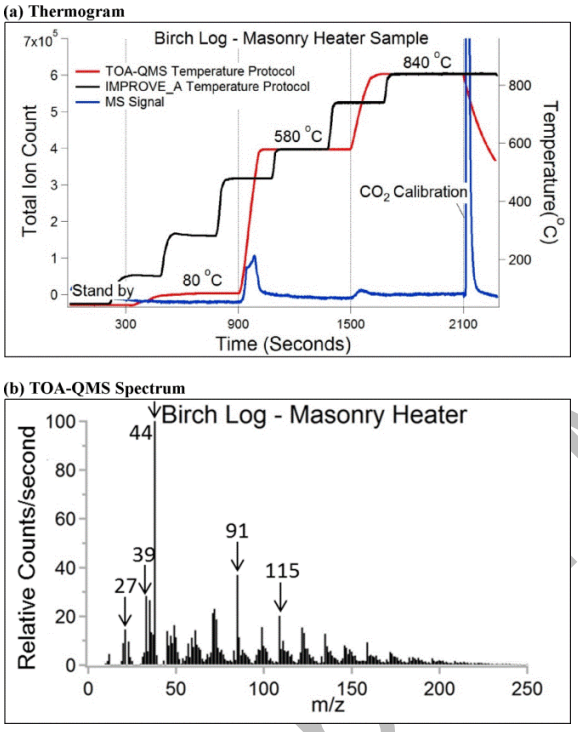

Figure 3. CO_2 ionization efficiency (Error bars of ± 1 standard deviation derived from replicate analyses are smaller than the size of the dots).

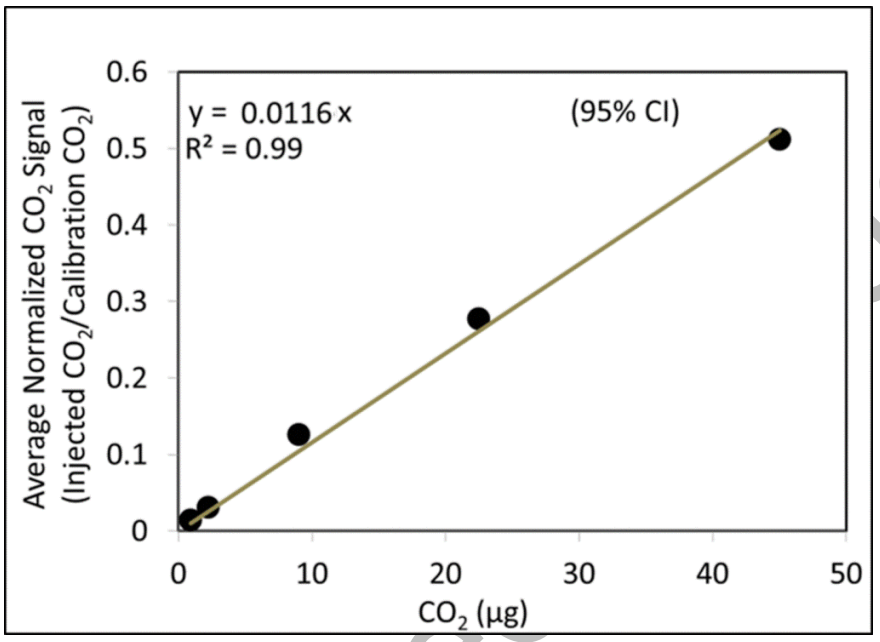

Figure 4. Calibration curves for: (a) ammonium, (b) nitrate, (c) sulfate, and (d) organic carbon using oxalic acid ($C_2H_2O_4$). Error bars indicates ± 1 standard deviation derived from replicates. The y-axis shows the corresponding summed species *m/z* signals from the TOA-QMS normalized using the CO_2 calibration peak *m/z* signal and divided by the filter punch area in cm^2. The x-axis values were obtained from quantification by IC and TOA analysis of portions of the filter standards. Linear regression curves are forced through zero.

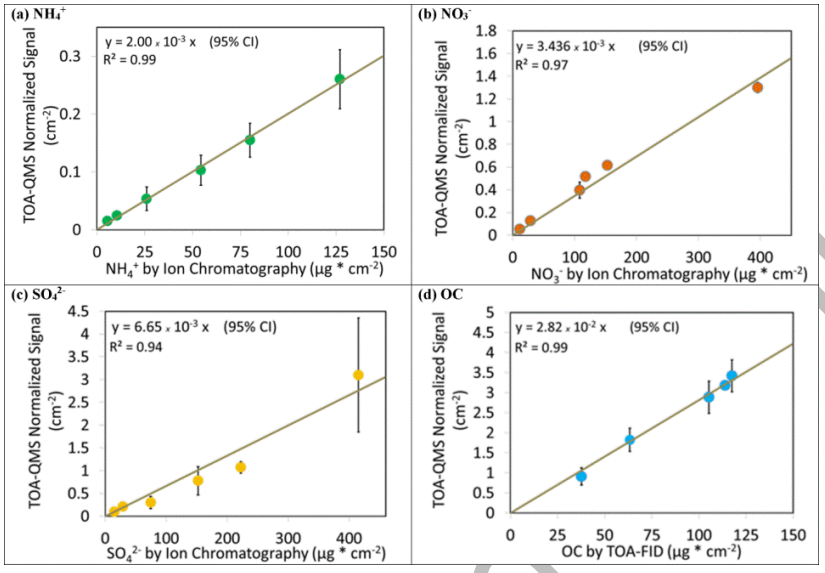

Figure 5. TOA-QMS and EI-AMS spectra for: (a) NH_4NO_3, with the most abundant peaks at *m/z* 14, 15, 16, 17, 18, 30, and 46; (b) $(NH_4)_2SO_4$, with the most abundant peaks observed at *m/z* 14, 15, 16, 17, 18, 32, 48, 64, 80, 81, and 98; (c) $C_2H_2O_4$ with the most abundant peaks for TOA-QMS at *m/z* 29, 44, 45, and 46, and for EI-AMS at *m/z* 16, 17, 27, 28, 43, 44, and 45; and (d) CO_2 with the most abundant peak at *m/z* 44.

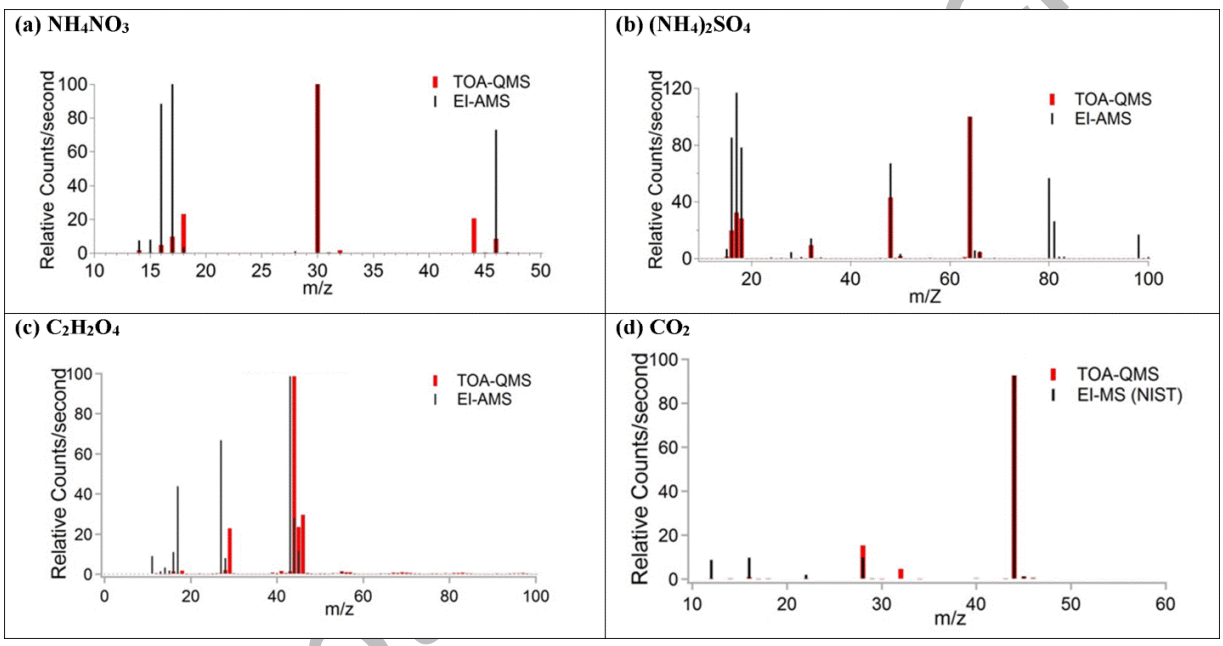

Figure 6. Spectrum processing flow diagram showing how interferences are removed from overlapping *m/z* signals.

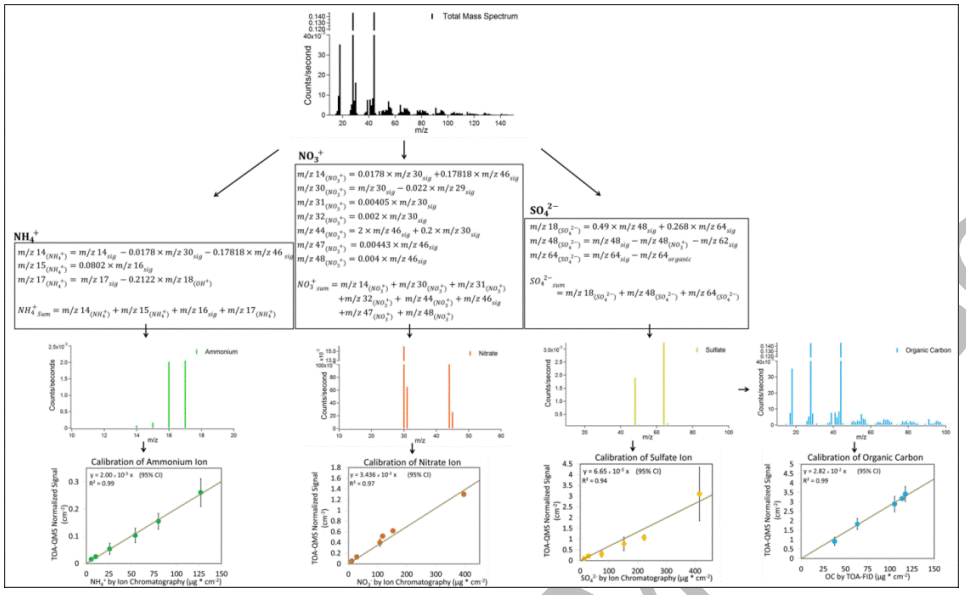

Figure 7. TOA-QMS concentrations vs: (a) NH_4^+ by IC; (b) NO_3^- by IC; (c) SO_4^{2-} by IC, and (d) OC by TOA for samples collected in Fresno, CA, and Baltimore, MD. Samples from the Western U.S., such as those from Fresno, CA are rich in NO_3^-, while samples from the Eastern U.S., such as those from Baltimore, are rich in SO_4^{2-}.

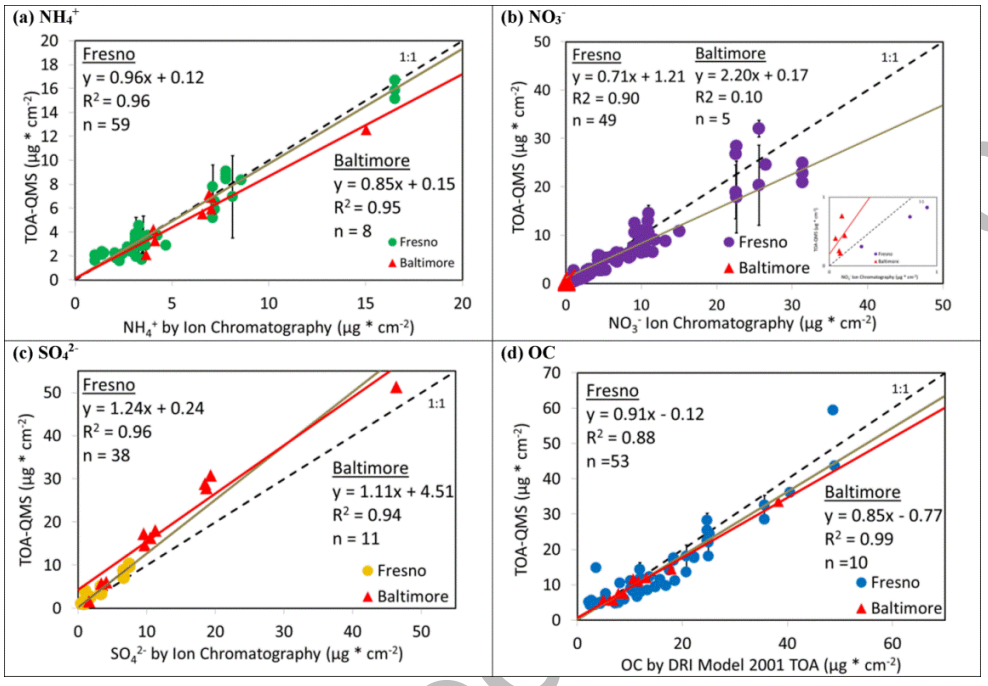

Figure 8. Average (colored bars) and standard deviations (black lines) of major chemical components in 58 Fresno, CA, samples measured by TOA-QMS, IC, and TOA. Elemental carbon (EC), soil, and salt concentrations determined from TOA, x-ray fluorescence (XRF), and atomic absorption spectrometry (AA), but not by TOA-QMS are included for completeness. The NO_3^- offset is apparent, but the low SO_4^{2-} averages are in reasonable agreement, as are the NH_4^+ and OC averages. The soil is calculated using the following formula: *Soil = 2.2Al + 2.49Si + 1.63Ca +1.94Ti + 2.42Fe* (Malm et al., 1994).

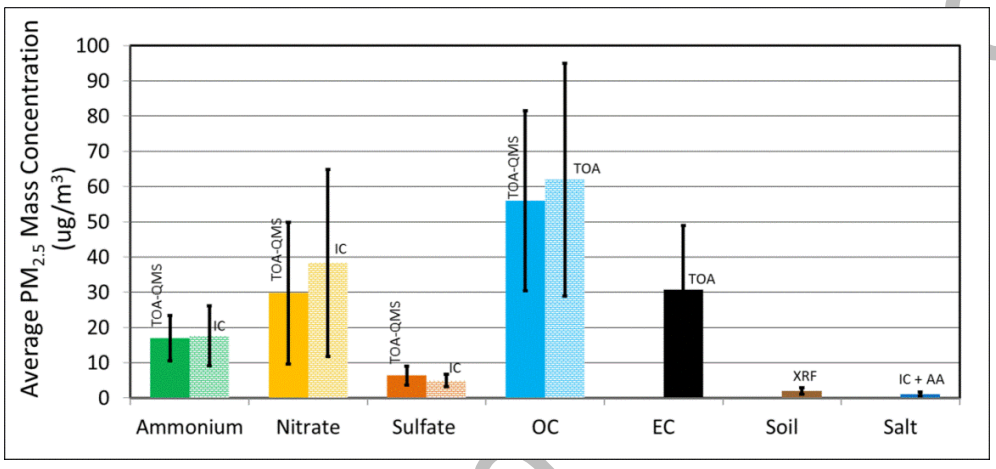

Figure 9. TOA-QMS mass concentration for: (a) NO_3^- by IC adjusted with a factor of 1.36 plotted vs. IC mass concentration; and (b) SO_4^{2-} by IC adjusted with a factor of 0.80.

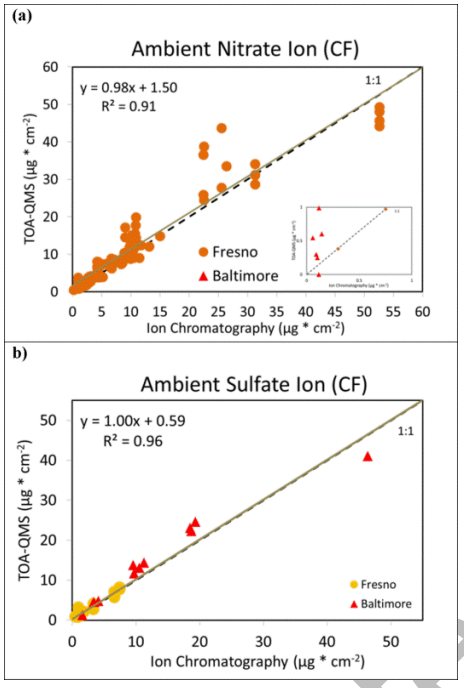

Figure 10. OC and ion contributions to $PM_{2.5}$ determined by TOA-QMS at the Fresno Supersite from 12/15/200 to 02/03/2001. Five samples were collected for each day (i.e., 0000-0500, 0500-1000, 1000-1300, 1300-1600, and 1600-2400 local standard time [LST]). Highest concentrations of OC and NO_3^- were observed during the late afternoon to night time period (1600-2400 LST).

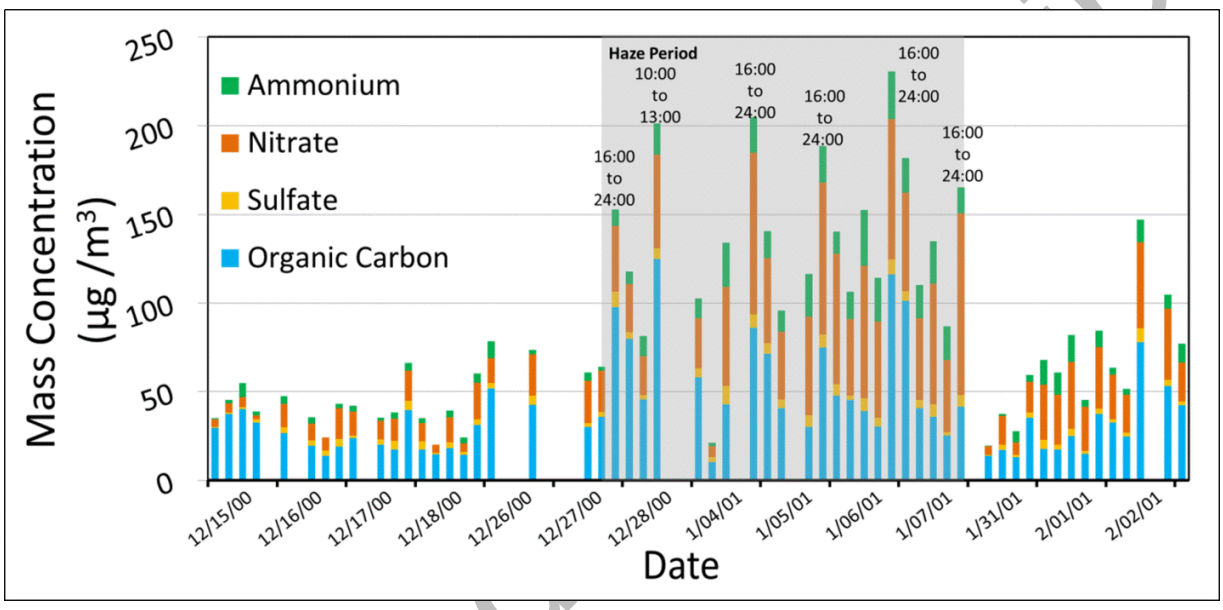

Table 1. Fragmentation patterns and interference corrections for ammonium, nitrate, and sulfate.

m/z	**Ion**	**Interference Ion**	**Calculation of Interference Ion**	**Corrected *m/z* signal for species**
Ammonium				
14	N^+	N^+ (from NO_3)	0.0178 x m/z 30[b] ($NO^+ \rightarrow N^+$) 0.17818 x m/z 46[b] ($NO_2^+ \rightarrow N^+$)	Signal at m/z 14 - Interference fragment
15	NH^+	Organic[c]	small interference from organic	0.0802 x m/z 16[b]
16	NH_2^+	Organic[c]	small interference from organic	Signal at m/z 16
17	NH_3^+	OH^+ (from	0.2122 x m/z 18[a]	Signal at m/z 17 - Interference

		H_2O)		fragment
Nitrate				
14	N^+	Organic[c]	small interference from organic	0.0178 x signal at m/z 30[b] + 0.17818 x signal at m/z 46[b]
30	NO^+	Organic at m/z 29	0.022 x m/z 29[a] (assumed organic)	Signal at m/z 30 - Interference fragment
31	NO^+	Organic[c]	small interference from organic	0.00405 x signal at m/z 30[a]
32	NO^+	Organic[c]	small interference from organic	0.002 x signal at m/z 30[a]
44	N_2O^+	Organic at m/z 44	small interference from organic	2 x signal at m/z 46 + 0.2 x signal at m/z 30[b]
46	NO_2^+	Organic[c]	small interference from organic	Signal at m/z 46

47	NO_2^+	Organic[c]	small interference from organic	0.00443 x signal at m/z 46[a]
48	NO_2^+	Organic[c]	small interference from organic	0.004 *x* signal at m/z 46[a]
Sulfate				
18	frag of SO_3	H_2O	small interference from organic	0.49 x signal at m/z 48[b] + 0.268 x signal at m/z 64[b]
48	SO^+	NO_2^+	nitrate at m/z 48 m/z 62 (assumed organic)	Signal at m/z 48 - Interference fragment
64	SO_2^+	Organic	0.5 x m/z 50[b] (assumed organic) 0.5 x m/z 78[b] (assumed organic)	Signal at m/z 64 - Interference fragment